LA-UR- 09-02145

Approved for public release; distribution is unlimited.

Title:	Modeling of the Nonlinear Resonant Response in Sedimentary Rocks
Author(s):	Vyacheslav O. Vakhnenko Oleksiy O. Vakhnenko James A. TenCate Thomas J. Shankland
Intended for:	Proceedings of the 16th International Congress on Sound and Vibration, Krakow, Poland 5-9 July 2009

Los Alamos
NATIONAL LABORATORY
EST. 1943

Form 836 (7/06)

The Sixteenth International Congress on Sound and Vibration
Kraków, 5-9 July 2009
ICSV16

MODELING OF THE NONLINEAR RESONANT RESPONSE IN SEDIMENTARY ROCKS

Vyacheslav O. Vakhnenko

Subbotin Institute of Geophysics, 63-B B.Khmel'nyts'ky Street, Kyiv 01054, Ukraine, e-mail: vakhnenko@ukr.net

Oleksiy O. Vakhnenko

Bogolyubov Institute for Theoretical Physics, 14-B Metrologichna Street, Kyiv 03143, Ukraine

James A. TenCate and Thomas J. Shankland

Los Alamos National Laboratory, Los Alamos, New Mexico 87545, USA

We suggest a model for describing a wide class of nonlinear and hysteretic effects in sedimentary rocks at longitudinal bar resonance. In particular, we explain: hysteretic behaviour of a resonance curve on both its upward and downward slopes; linear softening of resonant frequency with increase of driving level; gradual (almost logarithmic) recovery of resonant frequency after large dynamical strains; and temporal relaxation of response amplitude at fixed frequency. Starting with a suggested model, we predict the dynamical realization of end-point memory in resonating bar experiments with a cyclic frequency protocol. These theoretical findings were confirmed experimentally at Los Alamos National Laboratory.

1. Introduction

Sedimentary rocks, particularly sandstones, are distinguished by their grain structure in which each grain is much harder than the intergrain cementation material[1]. The peculiarities of grain and pore structures give rise to a variety of remarkable nonlinear mechanical properties demonstrated by rocks, both at quasistatic and alternating dynamic loading[1-4]. Thus, the hysteresis earlier established for the stress-strain relation in samples subjected to quasistatic loading-unloading cycles has also been discovered for the relation between acceleration amplitude and driving frequency in bar-shaped samples subjected to an alternating external drive that is frequency-swept through resonance. At strong drive levels there is an unusual, almost linear decrease of resonant frequency with strain amplitude, and there are long-term relaxation phenomena such as nearly logarithmic recovery (increase) of resonant frequency after the large conditioning drive has been removed.

In this report we present a short sketch of a model[5,6] for explaining numerous experimental observations seen in forced longitudinal oscillations of sandstone bars. According to our theory a broad set of experimental data can be understood as various aspects of the same internally consistent pattern[5,6]. Furthermore, the suggested theory will be shown to predict the dynamical realization of hysteresis with end-point memory, figuratively resembling its well-known quasistatic prototype[4,7,8].

TICKET NOT YET ISSUED. AIRFARE QUOTED IN ITINERARY IS NOT GUARANTEED UNTIL TICKETS ARE ISSUED.

You must use the USBank corporate card for all your rental car needs and decline the LDW/CDW coverage. For assistance call 505-667-4314 option 2 MON- FRI 8A -5P Emergency enroute call 800-787-1094 ID- S 7LB5 (After normal business hours) Official travel for Los Alamos National Laboratory Operated under contract for the United States Department of Energy It is your responsibility to call your travel reservationist and have them ask for a refund/credit if you cancel your trip. ***** Failure to do so could cause your account to become delinquent and hold up any reimbursement you might have coming to you.

Itinerary generated on Thu 04/02/2009 2:53 PM

2. Model of resonant oscillations

A reliable probing method widely applied in resonant bar experiments is to drive a horizontally suspended cylindrical sample with a piezoelectric force transducer cemented between one end of the sample and a massive backload, and to simultaneously measure the sample response with a low-mass accelerometer attached to the opposite end of the bar[2,4]. The evolution equation for the field of bar longitudinal displacements u as applied to above experimental configuration we write as follows

$$\rho\frac{\partial^2 u}{\partial t^2}=\frac{\partial\sigma}{\partial x}+\frac{\partial}{\partial x}\left[\frac{\partial\Im}{\partial(\partial^2 u/\partial x\partial t)}\right]. \tag{1}$$

Here we use the Stokes internal friction associated with the dissipative function $\Im=(\gamma/2)[\partial^2 u/\partial x\partial t]^2$. The quantities ρ and γ are, respectively, mean density of sandstone and coefficient of internal friction. The stress-strain relation $(\sigma-\partial u/\partial x)$ we adopt in the form

$$\sigma=\frac{E\operatorname{sech}\eta}{(r-a)\left[\cosh\eta\,\partial u/\partial x+1\right]^{a+1}}-\frac{E\operatorname{sech}\eta}{(r-a)\left[\cosh\eta\,\partial u/\partial x+1\right]^{r+1}}, \tag{2}$$

which for $r>a>0$ allows us to suppress the bar compressibility at strain $\partial u/\partial x$ tending toward $+0-\operatorname{sech}\eta$. Thus, the parameter $\cosh\eta$ is assigned for a typical distance between the centers of neighboring grains divided by the typical thickness of intergrain cementation contact.

The indirect effect of strain on Young's modulus E, as mediated by the concentration c of ruptured intergrain cohesive bonds, is incorporated in our theory as the main source of all nontrivial phenomena. We introduce a phenomenological relationship between defect concentration and Young's modulus. Intuition suggests that E must be some monotonically decreasing function of c, which can be expanded in a power series with respect to a small deviation of from its unstrained equilibrium value c_0. To lowest informative approximation we have

$$E=(1-c/c_{cr})E_+. \tag{3}$$

Here c_{cr} and E_+ are the critical concentration of defects and the maximum possible value of Young's modulus, respectively. The equilibrium concentration of defects c_σ associated with a stress σ is given by

$$c_\sigma=c_0\exp(\upsilon\sigma/kT), \tag{4}$$

where the parameter $\upsilon>0$ characterizes the intensity of dilatation. Although formula (4) should supposedly be applicable to the ensemble of microscopic defects in crystals, it was derived in the framework of continuum thermodynamic theory that does not actually need any specification of either the typical size of an elementary defect or the particular structure of the crystalline matrix. For this reason we believe it should also work for an ensemble of mesoscopic defects in consolidated materials, provided that for a single defect we understand some elementary rupture of intergrain cohesion. The approximate functional dependence of c_0 on temperature T and water saturation s based on experimental data was treated in refs.[5,6].

In order to achieve reliable consistency between theory and experiment we have used the concept of blended kinetics, which finds more-or-less natural physical justification in consolidated materials[6]. The idea presents the actual concentration of defects c as some reasonable superposition of constituent concentrations g, where each particular g obeys rather simple kinetics. Specifically, we take the constituent concentration g to be governed by the kinetic equation:

$$\partial g / \partial t = -[\mu\theta(g - g_\sigma) + \nu\theta(g_\sigma - g)](g - g_\sigma). \quad (5)$$

Here $\mu = \mu_0 \exp(-U/kT)$ and $\nu = \nu_0 \exp(-U/kT)$ are the rates of defect annihilation and defect creation, respectively, and $\theta(z)$ designates the Heaviside step function. A huge disparity $\nu_0 >> \mu_0$ between the priming rates (attack frequencies) ν_0 and μ_0 is assumed, notwithstanding the native cohesive properties of cementation material. Typical resonant response experiments[1,2,4] correspond to forced longitudinal vibration of a bar, which we associate with the boundary conditions:

$$u(x=0\,|\,t) = D(t)\cos(\varphi + \int_0^t d\tau\omega(\tau)), \quad \sigma(x=L\,|\,t) + \gamma\frac{\partial^2 u}{\partial x \partial t}(x=L\,|\,t) = 0, \quad (6)$$

where L is sample length, and $D(t)$ is driving amplitude. Initial conditions are

$$u(x\,|\,t=0) = 0, \quad \frac{\partial u}{\partial t}(x\,|\,t=0) = 0, \quad g(x\,|\,t=0) = c_0. \quad (7)$$

3. Computer simulation and comparison with experiment

Computer modeling of nonlinear and slow dynamics effects was performed in the vicinity of the resonance frequency $f_0(2)$, which we choose to be the second frequency ($l = 2$) in the fundamental set,

$$f_0(l) = \frac{2l-1}{4L}\sqrt{(1 - c_0/c_{cr})E_+/\rho} \qquad (l = 1,2,3,...). \quad (8)$$

Figure 1 shows typical resonance curves, i.e., dependences of response amplitudes R (calculated at $x = L$) on drive frequency $f = \omega/2\pi$, at successively higher drive amplitudes D. Solid lines correspond to conditioned resonance curves calculated after two frequency sweeps were performed at each driving level in order to achieve repeatable hysteretic curves. The dashed line illustrates an unconditioned curve obtained without any preliminary conditioning. Arrows on the three highest curves indicate sweep directions.

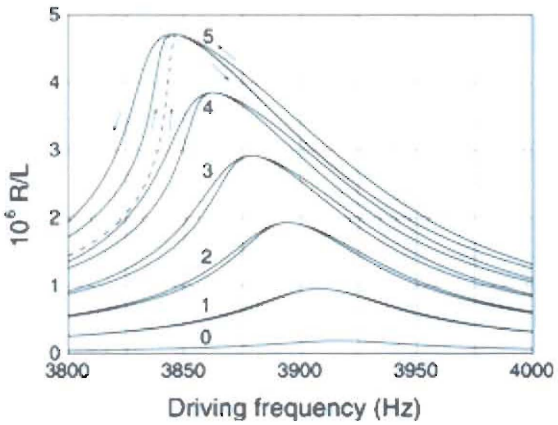

Figure 1. Resonance curves $j = 0,1,2,3,4,5$ at successively higher driving amplitudes $D_j = 3.8(j + 0.2\delta_{j0})10^{-8}L$. The time to sweep back and forth within the frequency interval 3700 – 4100Hz is chosen to be 120 s.

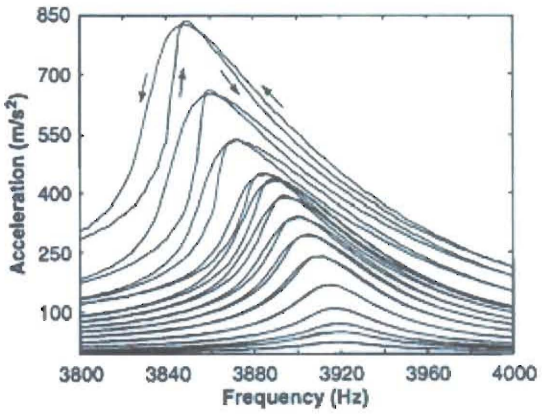

Figure 2. Experimental resonance curves (see reference[2]).

To improve the illustration, results of the computer simulations were adapted to experimental conditions appropriate to the data obtained by TenCate and Shankland for Berea sandstone[2]. In par-

ticular, $L = 0.3\,\mathrm{m}$, $f_0(2) = 3920\,\mathrm{Hz}$, $\upsilon E_+ / k \cosh\eta = 275\,\mathrm{K}$, $\cosh\eta = 2300$, $a = 2$, $r = 4$. For comparison the experimental resonance curves from ref.[2] are shown in Fig. 2. The shift of resonance frequency as a function of drive amplitude D was found to follow the almost linear dependence typical of materials with nonclassical nonlinear response, i.e., materials that possess all the basic features of slow dynamics (see refs.[5,6] for more details).

Apart from the reason mentioned earlier, measurements of temporal relaxation of acceleration amplitude at fixed frequency provide experimental documentation of how a rock gradually loses memory of the highest strain[2], and they thus elucidate the most interesting aspects of bond restoration kinetics. Figure 3 show theoretical relaxation curves that correctly reproduce the main features of the experiments (Fig. 4). As in the experiments the simulated response amplitude gradually decreased when the stopping frequency was lower than the resonant frequency (see Figs. 3(a), 3(b)) and increased when the stopping frequency was higher (see Figs. 3(c), 3(d)). Moreover, after approximately 10 min of relaxation the relaxation curves at a particular stopping frequency approached a long term level corresponding to the unconditioned part of the initial resonance curve whether or not the upward or downward preceding sweep was selected.

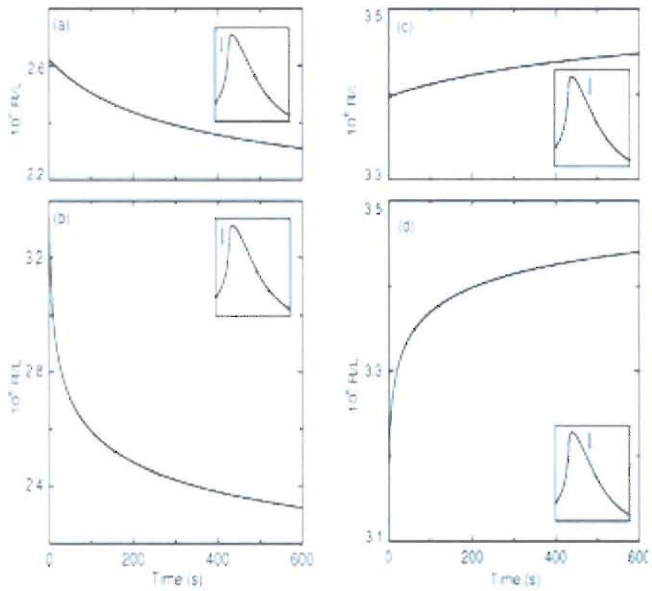

Figure 3. Response amplitude R at driving amplitude $D = 1.9 \cdot 10^{-7} L$ and fixed frequency (a,b) $f_s = 3825\,\mathrm{Hz}$, (c,d) $f_s = 3900\,\mathrm{Hz}$.

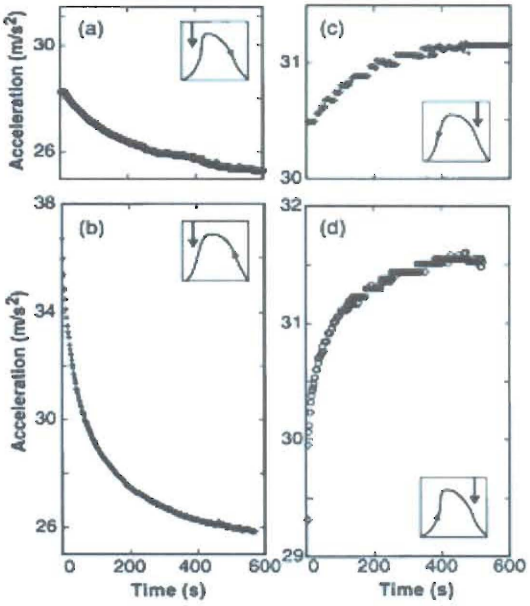

Figure 4. Experimental results from reference[2].

To reproduce another experimental facet of recovery time[2] we varied the previous simulations by stopping the sweep and simultaneously turning off the drive for 30 s with the sweep moving downward (Fig. 5(a)) or upward (Fig. 5(b)) from an already conditioned resonance. In a relatively short time (tens of seconds) the memory of the high strain amplitude rock had experienced at resonance diminished far more quickly than when the drive was left on. According to the kinetic Eq. (5) this distinction finds its rational explanation in a more favorable regime for defect annihilation under zero stress $\sigma = 0$ in comparison with the regime governed by the oscillating stress of a considerable amplitude (though lesser than that at resonance). Figure 5(a) displays the resonance curves obtained by the continuous sweep in upward followed by a sectionally continuous sweep downward. Figure 5(b) shows the complementary curves obtained by a continuous sweep downward followed by a sectionally continuous sweep upward. Effects of quick recovery (increase) of bar modulus E while sweep and drive were stopped are clearly seen as discontinuities in the curves. At stopping frequencies below resonance response amplitude drops closer to the first (recovered) upward-swept curve marked on Fig. 5(a) by the dashed line. At stopping frequencies above resonance

response amplitude jumps closer to the first (recovered) downward-swept curve marked in Fig. 5(b) by the dashed line.

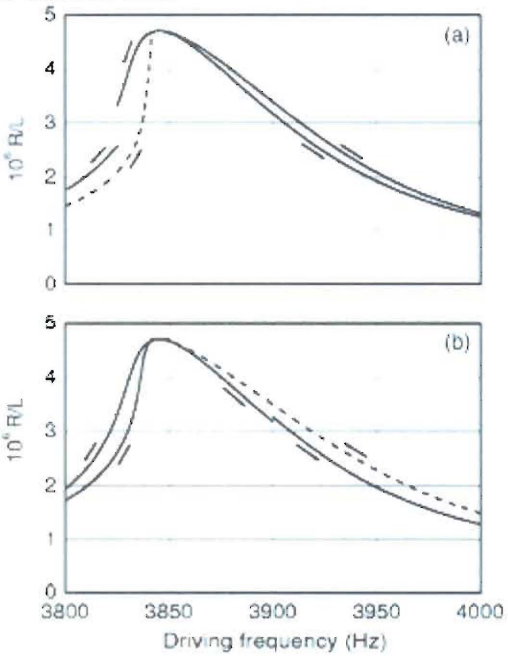

Figure 5. During the downward sweep both drive and sweep were turned off simultaneously for 30s at fixed frequency (a) $f_s = 3825\,\text{Hz}$, (b) $f_s = 3900\,\text{Hz}$.

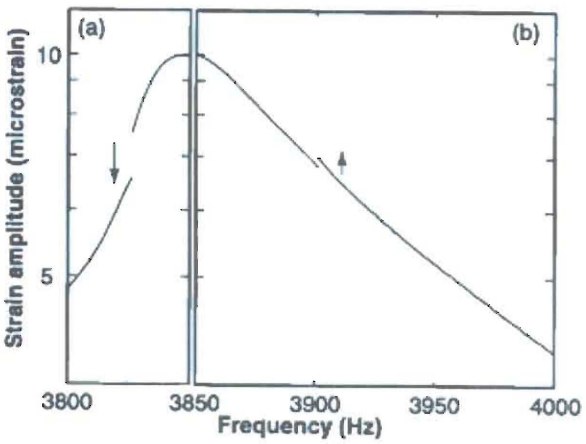

Figure 6. Experimental resonance curves (see reference[2]).

A qualitative view of these jumps comes from the indirect impact of strain on bar modulus through the concentration of defects. During the period of time when the sweep is approaching and passing resonance strain intensity becomes substantial causing a corresponding generation of defects, and the modulus decreases. This effect is manifested as a shift of resonance curve downward in frequency when the sweep has already passed resonance. If the drive and sweep are then turned off, the strain vanishes causing progressive annihilation of defects so that modulus increases. As a consequence the part of resonance curve, tracked after drive and sweep have been resumed, moves back (i.e., upward in frequency) as memory of the high strain is lost.

Figure 7 shows the gradual recovery of resonant frequency f_r to its maximum limiting value f_0 after the bar has been subjected to high amplitude conditioning and conditioning was stopped. We clearly see the very wide time interval $10 \le (t - t_c)/t_0 \le 1000$ of logarithmic recovery of the resonant frequency (Fig. 7), in complete agreement with experimental results[10] (Fig. 8). Here t_c is the moment when conditioning switches off and $t_0 = 1\text{s}$ is the time scaling constant. Curves $j = 1,2,3$ on lower Fig. 7 correspond to successively high water saturations $s_j = 0.05(2j-1)$.

4. Dynamical realization of end-point memory

The question of whether an effect similar to the end-point (discrete) memory that is observed in quasi-static experiments with a multiply-reversed loading-unloading protocol (see refs.[7-9] and references there) could also be seen in resonating bar experiments with a multiply-reversed frequency protocol has been raised in ref.[6] and was first examined theoretically. The graphical results of this investigation are presented in Fig. 9 (see also Fig. 16 in ref.[6]). The model constants are given in ref.[6]. One of the features of dynamical end-point memory, defined here as the memory of the

previous maximum amplitude of alternating stress, is seen as small loops inside the major loop. The starting and final points of each small loop coincide, which is typical of end-point memory.

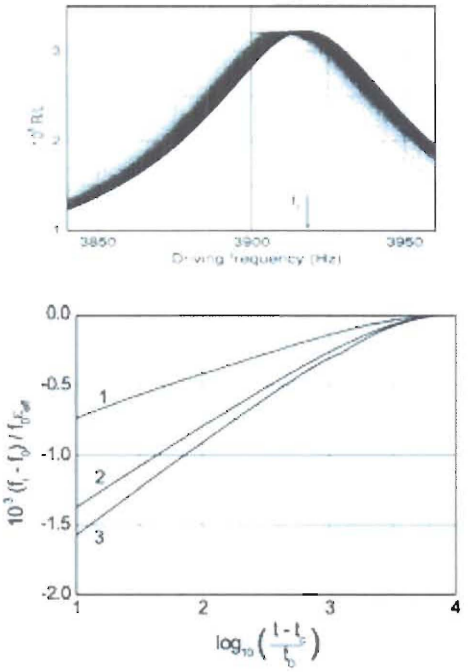

Figure 7. Recovery of resonant frequency f_r to its maximum limiting value f_0. Numerical result.

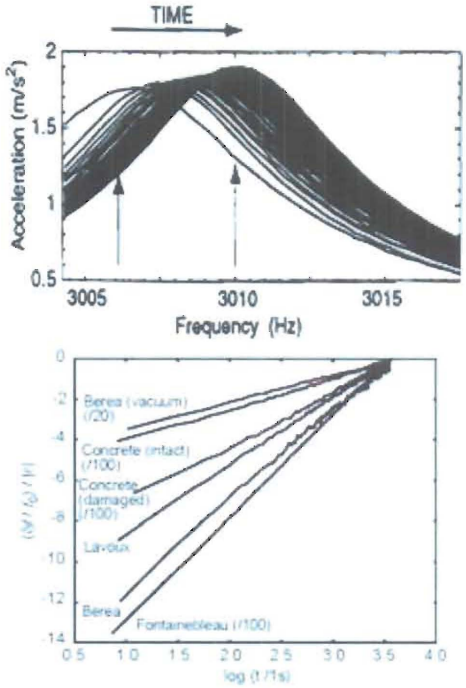

Figure 8. Recovery of resonant frequency f_r to its maximum limiting value f_0. Experimental results from reference[10].

Following the theoretical results, shown in Fig. 9, we performed experimental measurements to verify our prediction. The sample bar was a Fontainebleau sandstone and the drive level produced a calculated strain of about $2 \cdot 10^{-6}$ at the peak. Figure 10 shows the low frequency sides of resonance curves that correspond to the frequency protocol given on inset of Fig. 10. We clearly see that the beginning and end of each inner loop coincide, i.e., a major feature of end-point memory.

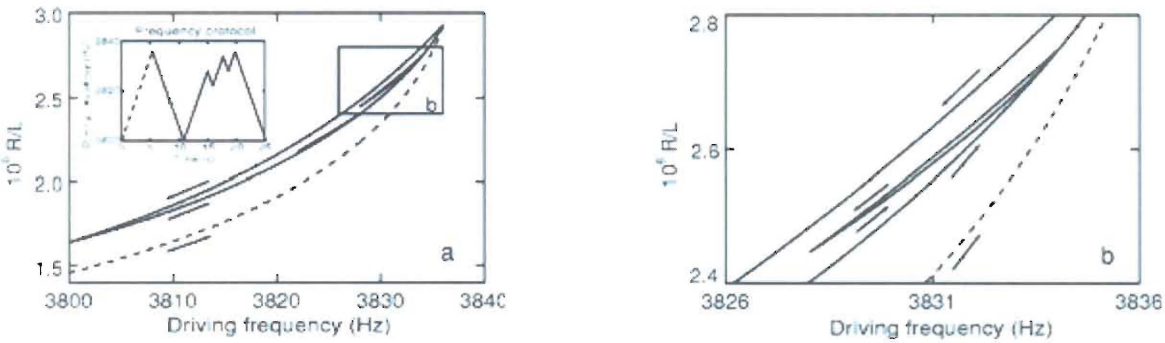

Figure 9. Manifestation of end-point memory in dynamic response with a multiply-reversed frequency protocol.

The experimental results for the Fontainebleau sandstone shown in Fig. 10 were reproduced by using our model equations though with constants (including a state equation) developed for Berea sandstone[5,6]. We note the good qualitative agreement between the experimental (Fig. 10) and the theoretical (Fig. 11) curves suggesting that our physical model is appropriate for both sandstones.

Hence, the suggested model enables us to describe correctly a wide class of experimental facts concerning the unusual dynamical behaviour of such mesoscopically inhomogeneous media as

sandstones. Moreover, as it is shown below, we have predicted the phenomenon of hysteresis with end-point memory in its essentially dynamical hypostasis. These theoretical findings were confirmed experimentally at Los Alamos National Laboratory.

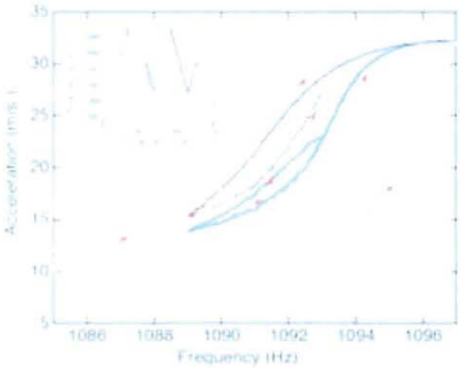

Figure 10. The low frequency sides of experimental resonance curves for Fontainebleau sandstone.

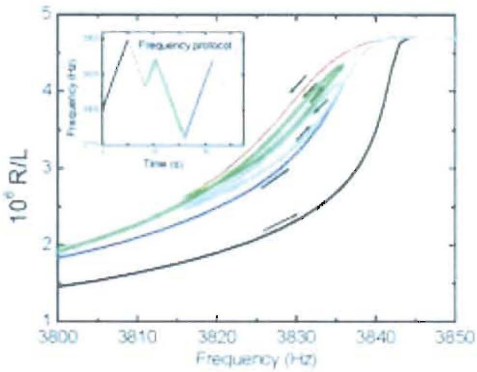

Figure 11. The low frequency sides of the resonance curves calculated for Berea sandstone

5. Acknowledgments

J.A.T. and T.J.S. thank the Geosciences Research Program, Office of Basic Energy Sciences of the U.S. Department of Energy for sustained assistance and also Institutional Funding support from the Los Alamos' LDRD program.

REFERENCES

1 R.A. Guyer, P.A. Johnson, Nonlinear mesoscopic elasticity: Evidence for a new class of materials, *Physics Today*, 1999, **52**, 30–35.

2 J.A. TenCate, T.J. Shankland, Slow dynamics in the nonlinear elastic response of Berea sandstone, *Geophys. Res. Lett.*, 1996, **23**, 3019–3022.

3 K. Van Den Abeele, J. Carmeliet, P. Johnson, B. Zinszner, The influence of water saturation on the nonlinear mesoscopic response of earth materials, and the implications to the mechanism of nonlinearity, *Journal of Geophysical Research*, 2002, **107**, 10,1029–10,1040.

4 J.A. TenCate, E. Smith, R.A. Guyer, Universal slow dynamics in granular solids, *Phys. Rev. Lett.*, 2000, **85**, 1020–1024.

5 O.O. Vakhnenko, V.O. Vakhnenko, T.J. Shankland, J.A. TenCate, Strain-induced kinetics of intergrain defects as the mechanism of slow dynamics in the nonlinear resonant response of humid sandstone bars, *Phys. Rev. E*, 2004, **70**, Repid communication, 015602(4).

6 O.O. Vakhnenko, V.O. Vakhnenko, T.J. Shankland, Soft-ratchet modelling of end-point memory in the nonlinear resonant response of sedimentary rocks, *Phys. Rev. B*, 2005, **71**, 174103(14).

7 R.A. Guyer, K.R. McCall, G.N. Boitnott, L.B. Hilbert Jr., T.J. Plona, Quantitative use of Preisach-Mayergoyz space to find static and dynamic elastic moduli in rock, *J. Geophys. Res.*, 1997, **102**, 5281–5293.

8 T.W. Darling, J.A. TenCate, D.W. Brown, B. Clausen, S.C. Vogel, Neutron diffraction study of the contribution of grain contacts to nonlinear stress-strain behaviour, *Geophys. Res. Lett.*, 2004, **31**, L16604(4).

9 V.O. Vakhnenko, O.O. Vakhnenko, J.A. TenCate, T.J. Shankland, Modeling of stress-strain dependences for Berea sandstone under quasistatic loading, *Phys. Rev. B*, 2007, **76**, 184108 (8).

10 J. A. TenCate, T. J. Shankland, Slow dynamics and nonlinear response at low strains in berea sandstone, in *Proceedings of the 16th International Congress on Acoustics and 135th Meeting of the Acoustical Society of America,* edited by P. A. Kuhl and L. A. Crum, New York: American Institute of Physics, 1998, **3**, 1565–1566 .